HHS Public Access

Author manuscript

Sci Transl Med. Author manuscript; available in PMC 2021 August 12.

Published in final edited form as:

Sci Transl Med. 2020 January 29; 12(528): . doi:10.1126/scitranslmed.aaw7905.

A dual apolipoprotein C-II mimetic-apolipoprotein C-III antagonist peptide lowers plasma triglycerides

Anna Wolska[1], **Larry Lo**[2], **Denis O. Sviridov**[1], **Mohsen Pourmousa**[3], **Milton Pryor**[1], **Soumitra S. Ghosh**[2], **Rahul Kakkar**[2], **Michael Davidson**[2], **Sierra Wilson**[1], **Richard W. Pastor**[3], **Ira J. Goldberg**[4], **Debapriya Basu**[4], **Steven K. Drake**[5], **Antony Cougnoux**[6], **Ming Jing Wu**[7], **Saskia B. Neher**[7], **Lita A. Freeman**[1], **Jingrong Tang**[1], **Marcelo Amar**[1], **Matt Devalaraja**[2,*,†], **Alan T. Remaley**[1,*,†]

[1]Lipoprotein Metabolism Laboratory, Translational Vascular Medicine Branch, National Heart, Lung, and Blood Institute, National Institutes of Health, Bethesda, MD, 20892, USA

[2]Corvidia Therapeutics, Inc., Waltham, MA, 02451, USA

[3]Laboratory of Computational Biology, National Heart, Lung, and Blood Institute, National Institutes of Health, Bethesda, MD, 20892, USA

[4]Division of Endocrinology, Diabetes and Metabolism, Department of Medicine, New York University School of Medicine, New York, NY, 10016, USA

[5]Critical Care Medicine Department, Clinical Center, National Institutes of Health, Bethesda, MD, 20892, USA

[6]Division of Translational Medicine, *Eunice Kennedy Shriver* National Institute of Child Health and Human Development, National Institute of Health, Bethesda, MD, 20892, USA

[7]Department of Biochemistry and Biophysics, University of North Carolina, Chapel Hill, NC, 27599, USA

Abstract

Recent genetic studies have established that hypertriglyceridemia (HTG) is causally related to cardiovascular disease, making it an active area for drug development. We describe a strategy for lowering triglycerides (TG) with an apolipoprotein C-II (apoC-II) mimetic peptide called D6PV that activates lipoprotein lipase (LPL), the main plasma TG-hydrolyzing enzyme, and antagonizes

[*]**Corresponding author:** aremaley1@nhlbi.nih.gov (A.T.R.), matt@corvidiatx.com (M.D.).
[†]These authors share senior authorship.

Author contributions: A.W.: conception and design, acquisition, analysis and interpretation of data, drafting and revising of manuscript; L.L.: conception and design, acquisition, analysis and interpretation of data, drafting and revising of manuscript; D.O.S.: conception and design, acquisition, analysis and interpretation of data, drafting and revising of manuscript; M.Pourmousa: acquisition, analysis and interpretation of data, drafting and revising of manuscript; M.Pryor: acquisition and analysis of data; S.S.G.: conception and design, acquisition, analysis and interpretation of data, revising of manuscript; R.K.: conception and design, revising of manuscript; M.Davidson: conception and design; revising of manuscript; S.W.: acquisition, analysis and interpretation of data, revising of manuscript; R.W.P.: analysis and interpretation of data, drafting and revising of manuscript; I.J.G.: analysis and interpretation of data; D.B.: acquisition and analysis of data; S.K.D.: acquisition, analysis and interpretation of data, revising the manuscript; A.C.: acquisition, analysis and interpretation of data, revising the manuscript; M.J.W.: acquisition, analysis and interpretation of data; S.B.N.: acquisition, analysis and interpretation of data, revising the manuscript; L.A.F.: acquisition, analysis and interpretation of data, drafting and revising of manuscript; J.T.: acquisition of data; M.A.: analysis of data, revising of manuscript; M.Devalaraja: conception and design, acquisition, analysis and interpretation of data, drafting and revising of manuscript; A.T.R.: conception and design, acquisition, analysis and interpretation of data, drafting and revising of manuscript.

the TG-raising effect of apoC-III. The design of D6PV was motivated by a combination of all-atom molecular dynamics simulation of apoC-II on the Anton 2 supercomputer, structural prediction programs, and biophysical techniques. Efficacy of D6PV was assessed ex vivo in human HTG plasma and was found to be more potent than full-length apoC-II in activating LPL. D6PV markedly lowered TG by more than 80% within a few hours in both apoC-II-deficient mice and h*APOC3*-transgenic (Tg) mice. In *hAPOC3*-Tg mice, D6PV treatment reduced plasma apoC-III by 80% and apoB by 65%. Furthermore, low-density lipoprotein (LDL) cholesterol did not accumulate but rather was decreased by 10% when h*APOC3*-Tg mice lacking the LDL-receptor (h*APOC3*-Tg x *Ldlr*$^{-/-}$) were treated with the peptide. D6PV lowered TG by 50% in whole-body inducible *Lpl* knockout (i*Lpl*$^{-/-}$) mice, confirming that it can also act independently of LPL. D6PV displayed good subcutaneous bioavailability of approximately 80% in nonhuman primates. Because it binds to high-density lipoproteins, which serve as a long-term reservoir, it also has an extended terminal half-life (42–50 h) in nonhuman primates. In summary, D6PV decreases plasma TG by acting as a dual apoC-II mimetic and apoC-III antagonist, thereby demonstrating its potential as a treatment for HTG.

One Sentence Summary:

An apolipoprotein C-II peptide mimetic for the treatment of hypertriglyceridemia activates lipoprotein lipase and blocks apolipoprotein C-III.

Introduction

Apolipoprotein C-II (apoC-II) plays a crucial role in triglyceride-rich lipoprotein (TRL) metabolism by activating lipoprotein lipase (LPL) (1–3), the primary plasma enzyme that hydrolyzes triglycerides (TG). Patients with familial hyperchylomicronemia (FC) with severe hypertriglyceridemia (HTG) due to mutations in genes involved in TG hydrolysis are at increased risk for pancreatitis (3). FC does not typically respond well to lipid-lowering therapies and thus represents an unmet clinical need (3, 4). Epidemiologic and genetic studies have revealed that patients with only moderately increased plasma TG are at increased risk of cardiovascular disease (CVD) (5, 6). Although the mechanistic link between plasma TG and CVD is not definitively established, it is likely related to the presence of cholesterol-enriched remnant lipoproteins, which can enter the blood vessel wall and trigger atherosclerosis (7).

Several new HTG therapies are in development (8), including anti-sense oligonucleotides to *APOC3*. ApoC-III inhibits LPL (9, 10) and blocks hepatic uptake of remnant lipoproteins (11). Monoclonal antibodies are also being developed against ApoC-III (12) and angiopoietin-like 3 (ANGPTL3), another LPL inhibitor (13). We have developed apoC-II mimetic peptides for decreasing plasma TG by activating LPL (14, 15). Our original peptides were designed based on the structure of human apoC-II, which contains 79 amino acids (16). The N-terminus of apoC-II forms a 26-amino acid long Type-A amphipathic helix that mediates binding to lipoproteins (17). The C-terminus contains a Type-G helix and is responsible for LPL activation (1, 18). Residues 40–57 between the two helices form a random coil (16, 19). Our first apoC-II mimetic peptide, 18A-CII, contained the C-terminal

helix of apoC-II, but the N-terminal helix was replaced by 18A (14), a synthetic helical peptide that was designed to bind tightly to lipoproteins (20, 21).

The 18A helix used in our original apoC-II mimetic peptide has no homology to any known human protein (21), thus raising the risk of immunogenicity. Based on structural insights gained from all-atom molecular dynamics (MD) simulations, we describe here a new peptide, called D6PV, which replaces 18A with a modified central region of apoC-II, while retaining the C-terminal LPL-activation domain. D6PV not only directly activates LPL but also blocks the ability of apoC-III to inhibit lipolysis and markedly lowers TG in human *APOC3*-transgenic (h*APOC3*-Tg) mice. D6PV also partially lowered TG in whole-body inducible *Lpl*-knockout (i$Lpl^{-/-}$) mice, indicating that it has TG-lowering effects independent of LPL. Pharmacokinetic (PK) studies in mice and nonhuman primates showed that D6PV has a relatively long terminal half-life of several days due to its ability to bind not only very low-density lipoproteins (VLDL), but also high-density lipoproteins (HDL), which serve as a long-term reservoir. Thus, we have revealed a new strategy for broadly treating HTG with a peptide that has dual apoC-II mimetic and apoC-III antagonist activity.

Results

MD simulation of apoC-II-lipid trilayer and peptide design

All-atom MD simulations were performed to gain insight into the interaction of apoC-II with lipids. A lipid trilayer, consisting of two layers of 1-palmitoyl-2-oleoyl-sn-glycero-3-phosphatidylcholine (POPC) surrounding a central layer of TG (3-palmitoyl-2-oleoyl-D-glycerol-1-linoleoyl), modelled the surface and neutral core lipids of TRL, respectively. Starting with a nuclear magnetic resonance (NMR) spectroscopy-derived structure (19, 22), apoC-II was placed on the top and bottom leaflets of the trilayer (Fig. 1A). Two simulations of 4.12 and 1 μs yielded structures for four apoC-II copies. Figure 1B shows snapshots for two copies in the longer simulation. The secondary structure (Fig. 1C) revealed three structurally distinct domains. Fig. 1D plots the distances of these three domains from the C2 atoms of the *sn*-2 acyl chains of phospholipids (fig. S1). The N-terminal region (~residues 13–39) of both copies of apoC-II was helical throughout the simulation and buried in POPC head groups, with average heights above the C2 atoms for the top and bottom copies of 3.2 ± 0.1 Å and 3.3 ± 0.2 Å, respectively ($t > 2.5$ μs). In contrast, the central region (~residues 40–57) was largely random coil and further from the C2 atoms. One copy contained several short helical segments, consistent with the relatively low helicity and predicted hydrophobic moment of the central region (Fig. 1E). The C-terminal region (~residues 58–79) for the top apoC-II copy (Fig. 1B) initially lost contact with lipids, adopted a condensed structure, and then re-associated with lipids after ~2.5 μs. The stability of the globular structure in this region stems from strong intra-peptide salt bridges (K76-D46, E78-K48, E78-K55, and E79-K55). This region also forms short and transient β-structures with the central domain (Fig. 1C).

The C-terminal region of the other apoC-II copy remained associated with lipids as an extended helix. The average heights of the C-terminal region of top and bottom copies above the C2 atoms were 7.7 ± 0.3 Å and 3.3 ± 0.3 Å, respectively ($t > 2.5$ μs). Thus, when in the extended configuration, the C-terminus is predicted to insert deeper into the lipid trilayer.

Consistent with the 4.12-μs simulation, the shorter 1-μs simulation (fig. S2, S3) also showed condensed and extended helices of the C-terminus. Overall, the MD simulations revealed that the N-terminal domain of apoC-II forms a long amphipathic helix that stably associates with lipids and the central domain is relatively unstructured. The C-terminal domain can form a helix that interacts with lipids or with the central domain, and accordingly adopts different types of secondary and tertiary structures.

Based on these structural insights, we engineered four new apoC-II mimetic peptides (D4, D5, D6, and D6PV) (Table 1) to replace the non-native 18A helix in 18A-CII. All new peptides lacked the N-terminal helix of apoC-II and started at the central random coil domain (residue 40). We introduced several amino acid substitutions into this region to increase its helicity and lipid binding properties. D6PV had the most substitutions and had a higher hydrophobic moment than 18A (Fig. 1E). An alanine to a proline replacement at position 19 provides a hinge between the two helices, and a methionine to a valine substitution at position 21 reduces potential oxidation. The predicted changes in free energy ($\Delta G_{transfer}$) for the interaction of D6PV and 18A-CII with lipids were similar (Table 2).

In an all-atom MD simulations (1 μs) of D6PV with a lipid trilayer (Fig. 2A), both copies remained helical and closely associated with lipids (fig. S4). D6PV caused a thinning of the phospholipid bilayers (Fig. 2B), and increased interdigitation of TG with the acyl chains of phospholipids (no peptide: 17.8 ± 0.2 mol%; D6PV: 21.0 ± 0.2 mol%, $P < 0.001$).

Circular dichroism (CD) spectroscopy indicated that D6PV was highly helical, particularly in the presence of 2,2,2-trifluoroethanol (TFE) (Fig. 2C). D6PV was more helical than the native random coil region linked with C-terminal helix of apoC-II (RCH2) (Fig. 2D), but less helical than D4, D5, and D6. Proline 19 (not present in the other peptides) likely interferes with hydrogen bonding of the D6PV backbone across the interhelical region and reduces its helicity.

The lipid binding properties of the peptides were assessed by a 1,2-dimyristol-sn-glycero-3-phosphatidylcholine (DMPC) vesicle clearance assay, which requires the peptide to bind and solubilize the lipid vesicle. The C-terminal helix of apoC-II (H2) by itself was ineffective. In contrast, D6PV had the best vesicle solubilization ability, followed by 18A-CII and RCH2 (Fig. 2E). The more structured helical peptides D4, D5, and D6 exhibited only modest activity. Like other strongly helical apolipoprotein mimetics, this may be due to peptide oligomerization at their hydrophobic faces, which limits interaction with lipids (20).

D6PV is a potent ex vivo activator of LPL in human plasma

D6PV was more potent in stimulating ex vivo lipolysis in apoC-II-deficient human plasma than full-length apoC-II (Fig. 3A, B). In contrast, H2 was almost completely inactive and RCH2 had only partial activity. Similar to 18A-CII (14, 15), D6PV increased LPL-dependent lipolysis in pooled plasma from patients with moderate HTG (Fig. 3C).

D6PV increases TG lipolysis in mouse models of HTG

Intraperitoneal (IP) injection of D6PV into apoC-II-deficient mice led to a rapid decrease of plasma TG, with a reduction of approximately 70% after 1 h and 85% after 3 h (Fig.

4A, fig. S5). TG did not return to baseline until 72 h (fig. S5), and there was no apparent hepatic toxicity after the treatment (Table S1). Plasma non-esterified fatty acids (NEFA) also decreased after peptide treatment (Fig. 4B), suggesting a rapid uptake of the released fatty acids by surrounding tissues and suppression of intracellular adipocyte lipolysis (23). D6PV also reduced TG after a bolus injection of Intralipid, an artificial TG emulsion (24), in both apoC-II-deficient (Fig. 4C) and C57Bl/6 (Fig. 4D) mice, indicating that apoC-II may be rate-limiting under certain physiological circumstances even in wild-type mice.

D6PV can displace apoC-III from lipoproteins

We hypothesized that the effect of D6PV in stimulating lipolysis in human HTG plasma (Fig. 3C) may be related to the antagonism of apoC-III. ApoC-III is known to raise plasma TG by inhibiting LPL activity (10), as well as by reducing hepatic uptake of TRL (25). Addition of apoC-III to human HTG plasma inhibited the ex vivo lipolysis of TG by approximately 40% (Fig. 5A), but D6PV completely prevented this inhibition at a molar ratio of 0.6:1 (D6PV:apoC-III). To explore the mechanism, we incubated human VLDL with varying concentrations of D6PV. The D6PV-VLDL mixture was then centrifuged through a 100 kDa-pore filter membrane to remove dissociated proteins. The VLDL-bound proteins were separated by sodium dodecyl sulfate polyacrylamide gel electrophoresis (SDS-PAGE) (Fig. 5B) and bands were identified by matrix-assisted laser desorption/ionization time-of-flight mass spectrometry (MALDI-TOF). D6PV caused a dose-dependent decrease in VLDL-bound apoC-III. There was also a decrease in other proteins bound to VLDL, including apoC-II, but the concomitant increase in bound D6PV should compensate for the loss of apoC-II in terms of LPL activation. D6PV can similarly displace apoC-III from HDL (fig. S6), which serves as a reservoir for this protein (11).

D6PV lowering of plasma TG in mice is partly LPL-independent

D6PV was then tested in h*APOC3*-Tg mice treated daily for 5 days (26). Plasma TG decreased 80% three hours after the first D6PV treatment (Fig. 6A). A comparable TG reduction was also observed on day 5 (Fig. 6A). In contrast, we observed only a 18% reduction in TG by 3 h in the vehicle control group, most likely because the mice were fasted for the first 6 h after the peptide or vehicle control treatment. D6PV also decreased total plasma apoC-III by approximately 85% (Fig. 6B), as well as apoC-III bound to VLDL (Fig. 6C), low-density lipoproteins (LDL) (Fig. 6D), and HDL (Fig. 6E). These results were confirmed by MALDI-TOF, which enabled the detection of the various glycoforms of human and mouse apoC-III and showed that human ApoC-III on VLDL was significantly reduced ($P < 0.05$) (fig. S7). Although variable, there was a marked increase in urinary apoC-III concentrations 1 and 3 h after D6PV injection (Fig. 6F). Plasma apoB also decreased by 3 h after peptide treatment by approximately 65% ($P < 0.01$) compared to baseline (26% compared to vehicle) (Fig. 6G). When the peptide was given to h*APOC3*-Tg x $Ldlr^{-/-}$ mice that lack the LDL-receptor (Fig. 6H), TG decreased to a similar degree as in h*APOC3*-Tg-treated mice (Fig. 6A) and LDL-cholesterol was approximately 10% lower after peptide treatment (fig. S8).

The above results are consistent with a mechanism whereby D6PV, independent of its direct effect in activating LPL, can lower TG by displacing apoC-III from TRL. The

displacement of apoC-III from TRL could reverse its inhibitory effect on LPL (Fig. 5A) or alternatively, by a potential LPL-independent mechanism, could also increase hepatic clearance of TRL before TRL can undergo complete lipolysis to LDL (27, 28). To test the latter possibility, i*Lpl*$^{-/-}$ mice were injected intravenously with the peptide. Plasma TG decreased by approximately 50% from baseline after 6 h (Fig. 6I). We obtained similar but slightly lower TG reduction after IP injection of D6PV into i*Lpl*$^{-/-}$ mice that had higher baseline TG (fig. S9A). We also observed a similar 50% reduction of TG after D6PV treatment in both i*Lpl*$^{-/-}$ and non-induced floxed *Lpl* (*Lpl*$^{fl/fl}$) mice, which still retain LPL but have a much lower baseline TG (fig. S9B). D6PV also decreased plasma NEFA in i*Lpl*$^{-/-}$ mice similar to what we observed in h*APOC3*-Tg mice (fig. S10). Overall, these results are consistent with the known LPL-independent effects of apoC-III in decreasing plasma clearance of TRL by hepatic uptake (11).

D6PV enhances ex vivo lipolysis of human HTG plasma samples

To determine whether the stimulation of ex vivo lipolysis by D6PV could serve as companion diagnostic to predict the in vivo response to the therapy, human plasma with TG ranging from 331 to 1669 mg/dL were tested (Fig. 7A). D6PV increased LPL-induced lipolysis for all samples (Fig. 7A). Total plasma apoC-III concentrations were positively associated with plasma TG ($R^2 = 0.7376$, $P = 0.003$). There appears to be an inverse trend between the degree of LPL activation and plasma TG ($R^2 = 0.1608$, $P = 0.2847$) similar to that previously seen with 18A-CII (14). However, no significant association was observed between the degree of LPL activation and total plasma apoC-III concentrations ($R^2 = 0.07014$, $P = 0.4910$). Furthermore, unlike C57Bl/6 mice, we were unable to improve ex vivo lipolysis after the addition of D6PV to mouse plasma from h*APOC3*-Tg mice (Fig. 7B), which is discordant with the in vivo mouse studies.

D6PV has a relatively long plasma half-life

Subcutaneously injected D6PV in apoC-II-deficient mice (Fig. 8A) acted similarly in lowering TG as when given IP (Fig. 4A). When D6PV was given SC (1, 10, and 100 mg/kg) (Fig. 8B) a dose-proportional increase in the maximum concentration (C_{max}) of D6PV in plasma was observed. In SC-administered animals plasma peptide levels peaked at 3 h (T_{max}) and the estimated bioavailability was over 65% for doses 1 and 10 mg/kg. The C_{max} concentration for D6PV (0.15 mg/mL) at a dose of 10 mg/kg BW, about half the dose used in our mouse studies (23.4 mg/kg BW), should be sufficient to maximally activate LPL based on our ex vivo sudies (Fig. 5A) and to displace apoC-III from VLDL (Fig. 5B). A nonlinear increase in the area-under-the-curve (AUC) was observed between the 10 and 100 mg/kg dose groups. The steady-state volume of distribution (V_{ss} of 81 mL/kg) was 60% larger than the plasma volume, indicating a relatively wide tissue distribution. The clearance rate was ~8 mL/kg/h, about 10% of the glomerular filtration rate, indicating that D6PV is not cleared renally. Although the elimination half-life for the initial phase ($t_{1/2,\alpha}$) after intravenous (IV) injection in mice was 3 h, the elimination half-life for the terminal phase ($t_{1/2,z}$), which is primarily due to its catabolism, was 9 h (fig. S11).

In nonhuman primates, D6PV was tested both by subcutaneous (SC) (Fig. 8C) and IV (fig. S11) dosing routes. A dose-proportional increase in C_{max} was observed after SC injection

and T_{max} was similar to mice. The SC bioavailability was approximately 80% for both doses, 8 and 80 mg/kg. A nonlinear increase in AUC between the 8 and 80 mg/kg SC dose groups is indicative of a two-compartment model. Consistent with mice, D6PV had a wide tissue distribution. The clearance rate at the 80 mg/kg dose was about 4-fold greater than the 8 mg/kg dose. This implies that when the plasma is saturated with the peptide, D6PV may undergo more rapid clearance. The terminal $t_{1/2,z}$ of D6PV after IV injection ranged from 42 to 50 h. Based on the PK properties of D6PV in mice and nonhuman primates, allometric scaling translates to a terminal half-life of approximately 3–4 days in humans.

The terminal half-life of most small peptides is typically much less than an hour due to peptide degradation and/or rapid renal clearance. The prolonged half-life of D6PV and its sustained TG-lowering effect in mice after a single dose could be explained by the binding to lipoproteins. To test this, we incubated fluorescent-tagged D6PV with pooled human HTG plasma and separated lipoproteins by fast-protein-liquid-chromatography (FPLC). The amount of phospholipids, which provides an approximation of lipoprotein surface, was similar for VLDL, LDL, and HDL (Fig. 8D). D6PV primarily bound to HDL and only a relatively small amount to VLDL (Fig. 8E). The equilibrium dissociation constant (K_d) of D6PV binding to HDL was determined to be 18.5 μM, whereas its affinity to VLDL was more than 10-fold lower (fig. S12). When the same plasma sample was supplemented with additional purified VLDL, a greater fraction of fluorescent D6PV was found on VLDL (Fig. 8E). When purified HDL pre-labelled with fluorescent D6PV was co-incubated with purified VLDL, D6PV transferred from HDL to VLDL, indicating that the lipoprotein-bound D6PV is in dynamic equilibrium between HDL and VLDL (Fig. 8F). In humans, HDL has a half-life of approximately 3 days (29), whereas VLDL and chylomicrons have half-lives of only a few hours (30). Thus, as has been shown for apoC-II (3), HDL can serve as a long-term reservoir for D6PV.

Because of the high affinity of D6PV for HDL, we investigated whether D6PV could interfere with the cholesterol efflux function of HDL. In fact D6PV by itself, similar to other apolipoprotein mimetic peptides (31), promoted ATP-Binding Cassette Transporter A1 (ABCA1)-mediated cholesterol efflux (fig. S13A) and also potentiated the cholesterol efflux ability of HDL (fig. S13B). This possibly occurs due to its ability to promote pre-beta HDL formation (fig. S13C) like other apolipoprotein mimetic peptides (32).

Discussion

The two major advances of this study are the design of a new apoC-II mimetic peptide primarily based on the native sequence of human apoC-II, and the finding that it lowers TG not only by activating LPL but also by antagonizing apoC-III. D6PV has a relatively good SC bioavailability and long plasma half-life and thus could potentially be developed as a once-a-week SC injectable therapy.

All-atom MD simulations revealed that the N-terminal helical domain of apoC-II is likely the main determinant for this protein’s ability to bind to lipoproteins (16). They also guided a strategy for substitution of amino acids in the central random coil region to improve its ability to bind lipids and serve as a replacement for the N-terminal helix. The use of

a proline hinge between the modified central region and the C-terminal LPL-activation domain enabled us to produce a truncated peptide that not only retained most of the parent apoC-II sequence, but also exhibited superior ex vivo and in vivo efficacy. A likely advantage of D6PV over 18A-CII is decreased immunogenicity, since D6PV is primarily based on the native apoC-II sequence and because short hydrophobic peptides that bind to lipids are relatively non-immunogenic (33).

The mechanism whereby apoC-II activates LPL is not well understood. It has been hypothesized that the rocking back and forth of its C-terminal helix in the phospholipid surface of TRL promotes the translocation of TG from the neutral lipid core to the surface where they can be hydrolyzed by LPL (19). Our simulation studies showed a thinning of the lipid trilayer and increased interdigitation of TG with acyl chains of phospholipids after D6PV binding, which may increase lipolysis by improving substrate availability. Another hypothesis is that there is a protein-protein interaction between the C-terminal helix of apoC-II and LPL itself, leading to an LPL conformational change and its activation (34). Because D6PV contains the last helical domain of apoC-II, such a protein-protein interaction also remains a possibility.

An unexpected finding is the ability of D6PV to not only lower TG in apoC-II-deficient mice but also in h*APOC3*-Tg mice. Based on both rare loss-of-function mutations (35) and common variants in large genome-wide association studies (36), apoC-III has been shown to be a major determinant of plasma TG and to be causally linked to CVD. Both anti-sense oligonucleotides (Volanesorsen) (37) and monoclonal antibodies (12) against apoC-III have been investigated as possible therapies. In a phase III study, Volanesorsen decreased plasma TG by as much as 77% in patients with FC and was also partially effective in LPL-deficient patients (38), which is consistent with what we observed in our i$Lpl^{-/-}$ mouse studies. In addition to decreasing plasma apoC-III, Volanesorsen also lowers apoC-II by about half, most likely due to enhanced hepatic clearance of TRL that carry both proteins (39). Since several studies have shown that the ratio between apoC-III and apoC-II may be critical for lipolysis and TG clearance (40, 41), the lowering of plasma apoC-II by Volanesorsen may partially limit its effectiveness in decreasing TG. D6PV, in contrast, effectively replenishes the loss of any apoC-II.

In h*APOC3*-Tg mice, D6PV lowered total plasma apoC-III to a similar degree as Volanesorsen (39). Compared to other exchangeable apolipoproteins, apoC-III has relatively weak lipoprotein binding (42), which may account for its displacement from VLDL and HDL after D6PV treatment. This finding is also consistent with natural mutations in the amphipathic helical regions of apoC-III that lead to its increased renal clearance (12). The decrease in apoC-III on TRL then likely leads to a reversal of inhibition of LPL as we observed in our ex vivo lipolysis, which may then trigger further dissociation of apoC-III from TRL due to the build-up of fatty acids and increased surface tension from lipolysis (3, 42). The ability of D6PV to lower TG in i$Lpl^{-/-}$ mice indicates that it can also work through an LPL-independent pathway, most likely involving enhanced hepatic clearance of TRL due to a decrease in apoC-III (27, 28). Any residual apoC-III still on the partially lipolyzed TRL could then be removed by holoparticle hepatic uptake, which likely accounts for the decrease in apoB we observed after D6PV treatment in h*APOC3*-Tg mice. The fact that

D6PV similarly lowered TG in h*APOC3*-Tg x $Ldlr^{-/-}$ mice and LDL-C did not accumulate, indicates that the clearance of partially lipolyzed TRL depends on other receptors besides the LDL receptor. The relative contribution of the 3 potential mechanisms for TG lowering by D6PV (I. Direct LPL activation, II. Reversing inhibition of LPL by displacing apoC-III from TRL, and III. LPL-independent pathway by enhancing hepatic clearance of TRL) likely varies in our different animal models and possibly in humans, depending on the TG level, the ratio of apoC-II to apoC-III and the availability of LPL.

Although TG are primarily transported by apoB-containing lipoproteins, we observed that D6PV most avidly bound to HDL. Because of its high curvature, which causes packing defects in its phospholipid surface, HDL tightly binds many different types of proteins, including apoC-II and apoC-III (43). In the case of D6PV, this may be beneficial, because it extends its plasma half-life, by allowing HDL to serve as a long-term reservoir for the peptide, like it does for apoC-II (3). As newly secreted chylomicrons or VLDL particles enter the circulation, we hypothesize that D6PV transfers from HDL to these TRL particles to promote their lipolysis like we observed in our in vitro binding studies. Importantly, the binding of D6PV to HDL did not, at least based on in vitro assays, interfere with the ability of HDL to efflux cholesterol but rather enhanced it.

ApoC-II deficiency is a promising indication for D6PV based on the observation that it had a sustained effect in markedly lowering plasma TG in apoC-II-deficient mice. There are currently no specific treatments for this rare genetic disorder except dietary therapy (3). The dual pharmacology of D6PV in functioning as both an apoC-II mimetic and an apoC-III antagonist also makes it an attractive candidate for generalized HTG for the prevention of CVD, particularly if it can also lower apoB, which appears to be the case, at least in our mouse studies.

There are several hurdles, however, before D6PV can be developed into a therapy. First, its long-term TG-lowering effect and toxicology profile need to be assessed in nonhuman primates to more fully determine its efficacy and safety prior to testing in human subjects. In addition, although D6PV is largely based on the native human apoC-II sequence, it contains several amino acid substitutions and thus may still elicit an immune response. It is difficult, however, to assess this in preclinical studies because translation of immunogenicity findings in animal models to humans is unpredictable. Finally, more studies are needed to fully understand the mechanism of action of the peptide, particularly in regard to its LPL-independent effect, by testing it in additional animal models lacking apoC-III and hepatic TRL receptors (27).

In summary, we described a therapeutic strategy for decreasing plasma TG with an apoC-II mimetic peptide that activates LPL and antagonizes the TG-raising effects of apoC-III. Feasibility was shown in multiple animal models of HTG, thus providing strong support for further research and development.

Material and Methods

Study design

The objective was to develop an apoC-II mimetic peptide that promotes the lipolysis of TRL. We designed a new apoC-II mimetic peptide based on the native structure of human apoC-II; examined its structural and biophysical properties; tested its activity in promoting TG lipolysis in human HTG plasma and in HTG mouse models; and evaluated its bioavailability and half-life in mice and nonhuman primates. Mice were randomized based on their age, sex, weight, and plasma TG concentrations. Numbers of mice were based on magnitude of observed changes and variability in the results and are specified in figure legends. All mouse studies were approved by the NHLBI Animal Care and Use Committee (ACUC) (protocol # H-0050), New York University School of Medicine ACUC (protocol # 160810), or University of North Carolina ACUC (protocol # 17–115.0-C). The nonhuman primate (*Cynomolgus monkey*) single-dose PK study was done at MPI Research Inc. (Mattawan, MI) and the mouse PK study at HD Biosciences (San Diego).

Peptide chemistry and analysis

Peptides were synthesized by Peptide 2.0, using standard 9-fluorenylmethoxycarbonyl chemistry and purified to greater than 95% homogeneity by reverse-phase high-performance liquid chromatography (HPLC). Peptides were dissolved in 238 mM Trehalose and 20 mM Tris buffer (TT buffer), pH 8.2. A fluorescent version of D6PV was synthesized by adding 5-TAMRA to the N-terminal amino group. Peptide concentrations in plasma were measured by liquid chromatography with tandem mass spectrometry (LC-MS/MS). D6PV and an internal standard (IS; Delta6PL) were extracted from 50 μL of EDTA-plasma by protein precipitation, using 3:1 acetonitrile (ACN):methanol (MeOH). After evaporation and reconstitution, extracts were analyzed by LC-MS/MS. The lower limit of quantitation was 0.2 μg/mL. The calibration curve was linear from 0.2 to 40 μg/mL. Additional details of peptide studies are available in supplementary materials (Peptide chemistry and analysis).

MD simulations

Four simulations of systems containing POPC, TG, D6PV, and apoC-II were performed; see table S2 for compositions and trajectory lengths. A lipid trilayer consisting of 128 TG molecules surrounded by two layers of 80 POPC molecules mimicked the core and surface lipids of VLDL. The trilayer was assembled (44) and hydrated with water and 150 mM sodium chloride (NaCl). The area per POPC converged after 700 ns of the 1 μs simulation (fig. S14). A simulation frame from the last 300 ns with the area per POPC close to the average value yielded a representative equilibrated trilayer. After removing solvent molecules, two copies of either D6PV or apoC-II, one per POPC leaflet, were placed on the equilibrated trilayer with their hydrophobic sides facing the interior. Systems were hydrated with water and 150 mM NaCl.

The initial structures of peptides as extended helices were developed using CHARMM (45). Initial conformations of apoC-II on each leaflet corresponded to models 1 and 4 of the NMR structures in dodecyl phosphocholine (DPC) (19). To ensure sufficient sampling, an additional simulation was carried out starting from models 3 and 13 of apoC-II in DPC

(19) and sodium dodecyl sulfate (SDS) (22), respectively. The first 12 residues of apoC-II are missing in both NMR models and thereby absent in the simulations. The D6PV-trilayer system was simulated for 1 μs and the apoC-II-trilayer systems for 4.12 μs and 1 μs, respectively. The trilayer and peptide simulations were performed on an in-house computer cluster (Biowulf) and apoC-II on Anton 2. Additional details are available in supplementary materials (Simulation details).

Animal studies

C57Bl/6 (all female, 5–6 months old) (Taconic Biosciences, Inc.), apoC-II-deficient (female and male, 7–12 months old) (15), h*APOC3*-Tg (female and male, 4–9 months old) (26), h*APOC3*-Tg x $Ldlr^{-/-}$ (female and male, 7–10 months old) (46), and i$Lpl^{-/-}$ (all male, 6–21 months old) and non-induced $Lpl^{fl/fl}$ (all male, 21 months old) (27, 47) mice were fed a regular rodent chow diet (NIH-31 chow diet: Zeigler Brothers, Inc.) and were treated with D6PV [4.7, 23.4, or 46.7 mg/kg body weight (BW)] in TT buffer or with TT buffer alone (vehicle control) by the indicated route. Mice treated with 20% Intralipid (24) were given either 0.6 mL or 1 mL by bolus IP injection. Blood samples were obtained from the retroorbital plexus.

For the nonhuman primate (*Cynomolgus monkey*; all male, age 2.5–4.5 years old, 2–6 kg) single-dose PK study, 12 *Cynomolgus monkeys* were assigned into 4 groups, 2 doses (8 and 80 mg/kg) and 2 dose routes (SC and IV), with 3 animals in each group. Each animal received a single dose of D6PV administered IV or SC on day one. IV doses were administered via the saphenous vein. SC doses were administered via bolus injection between the skin and underlying tissue in the scapular region.

For the mouse single-dose PK study, 72 C57Bl/6 mice (all female, 2 months old) were assigned into 4 groups, 3 doses (1, 10, and 100 mg/kg) and 2 dose routes (SC and IV), with 18 animals in each group. Each animal received a single dose of D6PV SC or IV on day one. Plasma samples were collected at pre-specified time points and D6PV was measured by LC-MS/MS.

Analyses of plasma lipids and lipoproteins

Plasma lipids and NEFA were measured enzymatically (FUJIFILM Wako Diagnostics) (15). LPL activity was determined by measuring the generation of NEFA as described in supplementary materials (LPL activity assay). Human apoC-III and mouse apoB were measured by enzyme-linked immunosorbent assays (Cell Biolabs, Inc. for human apoC-III and Abcam for mouse apoB). To investigate apoC-III displacement by D6PV, human VLDL (TG=291 mg/dL) were isolated by density gradient ultracentrifugation (d=1.009–1.019 g/mL) and incubated with the indicated concentrations of D6PV for 1 h at 37°C. The reaction mixture was centrifuged in 100-kDa cutoff spin filters (Millipore) and washed 3 times with phosphate buffered saline (PBS) to remove apolipoproteins dissociated from VLDL after D6PV treatment. VLDL were recovered from the spin columns and bound apolipoproteins were separated by electrophoresis on 4–12% NuPAGE Bis-Tris Protein gels (ThermoScientific). After staining with Coomassie Blue, proteins were extracted and identified by MALDI-TOF, as described in supplementary materials (MALDI-TOF analysis

of plasma). HDL studies were similarly performed using HDL isolated by FPLC (AKTA pure, GE Scientific) on Superose 6 tandem columns (GE Scientific) from h*APOC3*-Tg mice.

Statistical analysis

Experimental and simulation results are presented as mean ± standard deviation (S.D.). PK of plasma peptide concentrations were analyzed by a multi-compartmental model with WinNonLin software (Certara Inc.). Statistical tests were performed with GraphPad PRISM version 5.0 software. Raw data are provided in data file S1.

Supplementary Material

Refer to Web version on PubMed Central for supplementary material.

Acknowledgments:

The authors thank Dr. Piszczek from NHLBI-Biophysics Core Facility for technical support, Dr. Dong from University of Pittsburgh School of Medicine for h*APOC3*-Tg mice, and Dr. Glew from University of New Mexico for editing the manuscript. Anton 2 computer time was provided by the Pittsburgh Supercomputing Center (PSC) through NIH-Grant R01GM116961. The Anton 2 machine at PSC was generously made available by D.E. Shaw Research. This work also utilized computational resources of the NIH-HPC Biowulf cluster.

Funding: Research was supported by the Intramural Research Program of the NHLBI at the National Institutes of Health and a research grant from Corvidia Therapeutics, Inc., Waltham, MA, USA. M.J.W. and S.B.N. were supported by grants 1R01HL125654 and 550KR171713. I.J.G. was supported by HL45095 and HL73029.

Competing interests: A.W., L.L., D.O.S., S.S.G., M.Devalaraja, and A.T.R. are co-inventors on US patent application PCT/US2018/014532, 107102123, submitted by Corvidia Therapeutics Inc. that covers composition and use of apoC-II mimetic peptides described in this paper. A.T.R. and M.A. are co-inventors on US patent #8,936,787 held by the National Institutes of Health that covers composition and use of 18A-CII mimetic peptide. A.W., D.O.S., and A.T.R. have a research grant HL-CR-16-005 with Corvidia Therapeutics, Inc., Waltham, MA, USA. L.L., S.S.G., R.K., M.Davidson, and M.Devalaraja are employed by Corvidia Therapeutics, Inc., Waltham, MA, USA. R.K., M.Davidson, and M.Devalaraja are stock holders of AstraZeneca. M.Pourmousa, M.Pryor, S.W., R.P., I.J.G., D.B., S.K.D., A.C., M.J.W., S.B.N., L.A.F., and J.T declare no conflicts of interest.

Data and materials availability:

All data associated with this study are present in the paper or in the Supplementary Materials.

References:

1. Shen Y, Lookene A, Nilsson S, Olivecrona G, Functional analyses of human apolipoprotein CII by site-directed mutagenesis: Identification of residues important for activation of lipoprotein lipase. Journal of Biological Chemistry277, 4334–4342 (2002)10.1074/jbc.M105421200).
2. Lewis GF, Xiao C, Hegele RA, Hypertriglyceridemia in the genomic era: A new paradigm. Endocrine Reviews36, 131–147 (2015)10.1210/er.2014-1062). [PubMed: 25554923]
3. Wolska A, Dunbar RL, Freeman LA, Ueda M, Amar MJ, Sviridov DO, Remaley AT, Apolipoprotein C-II: New findings related to genetics, biochemistry, and role in triglyceride metabolism. Atherosclerosis267, 49–60 (2017); published online EpubDec (10.1016/j.atherosclerosis.2017.10.025). [PubMed: 29100061]
4. Gotoda T, Shirai K, Ohta T, Kobayashi J, Yokoyama S, Oikawa S, Bujo H, Ishibashi S, Arai H, Yamashita S, Harada-Shiba M, Eto M, Hayashi T, Sone H, Suzuki H, Yamada N, R. o. M. a. I. D. b. t. M. o. H. L. Research Committee for Primary Hyperlipidemia JWelfare in, Diagnosis and management of type I and type V hyperlipoproteinemia. J Atheroscler Thromb19, 1–12 (2012). [PubMed: 22129523]

5. Toth PP, Granowitz C, Hull M, Liassou D, Anderson A, Philip S, High Triglycerides Are Associated With Increased Cardiovascular Events, Medical Costs, and Resource Use: A Real-World Administrative Claims Analysis of Statin-Treated Patients With High Residual Cardiovascular Risk. J Am Heart Assoc7, e008740 (2018); published online EpubAug 7 (10.1161/JAHA.118.008740). [PubMed: 30371242]

6. Nordestgaard BG, Triglyceride-Rich Lipoproteins and Atherosclerotic Cardiovascular Disease: New Insights From Epidemiology, Genetics, and Biology. Circ Res118, 547–563 (2016); published online EpubFeb 19 (10.1161/CIRCRESAHA.115.306249). [PubMed: 26892957]

7. Peng J, Luo F, Ruan G, Peng R, Li X, Hypertriglyceridemia and atherosclerosis. Lipids Health Dis16, 233 (2017); published online EpubDec 6 (10.1186/s12944-017-0625-0). [PubMed: 29212549]

8. Larsen LE, Stoekenbroek RM, Kastelein JJP, Holleboom AG, Moving Targets: Recent Advances in Lipid-Lowering Therapies. Arterioscler Thromb Vasc Biol39, 349–359 (2019); published online EpubMar (10.1161/ATVBAHA.118.312028). [PubMed: 30676072]

9. Gaudet D, Brisson D, Tremblay K, Alexander VJ, Singleton W, Hughes SG, Geary RS, Baker BF, Graham MJ, Crooke RM, Witztum JL, Targeting APOC3 in the familial chylomicronemia syndrome. N Engl J Med371, 2200–2206 (2014); published online EpubDec 04 (10.1056/NEJMoa1400284). [PubMed: 25470695]

10. Brown WV, Baginsky ML, Inhibition of lipoprotein lipase by an apoprotein of human very low density lipoprotein. Biochem Biophys Res Commun46, 375–382 (1972); published online EpubJan 31 ([PubMed: 5057882]

11. Kohan AB, Apolipoprotein C-III: a potent modulator of hypertriglyceridemia and cardiovascular disease. Current opinion in endocrinology, diabetes, and obesity22, 119–125 (2015); published online EpubApr (10.1097/med.0000000000000136).

12. Khetarpal SA, Zeng X, Millar JS, Vitali C, Somasundara AVH, Zanoni P, Landro JA, Barucci N, Zavadoski WJ, Sun Z, de Haard H, Toth IV, Peloso GM, Natarajan P, Cuchel M, Lund-Katz S, Phillips MC, Tall AR, Kathiresan S, DaSilva-Jardine P, Yates NA, Rader DJ, A human APOC3 missense variant and monoclonal antibody accelerate apoC-III clearance and lower triglyceride-rich lipoprotein levels. Nat Med23, 1086–1094 (2017); published online EpubSep (10.1038/nm.4390). [PubMed: 28825717]

13. Wang Y, Gusarova V, Banfi S, Gromada J, Cohen JC, Hobbs HH, Inactivation of ANGPTL3 reduces hepatic VLDL-triglyceride secretion. J Lipid Res56, 1296–1307 (2015); published online EpubJul (10.1194/jlr.M054882). [PubMed: 25954050]

14. Amar MJ, Sakurai T, Sakurai-Ikuta A, Sviridov D, Freeman L, Ahsan L, Remaley AT, A novel apolipoprotein C-II mimetic peptide that activates lipoprotein lipase and decreases serum triglycerides in apolipoprotein E-knockout mice. J Pharmacol Exp Ther352, 227–235 (2015); published online EpubFeb (10.1124/jpet.114.220418). [PubMed: 25395590]

15. Sakurai T, Sakurai A, Vaisman BL, Amar MJ, Liu C, Gordon SM, Drake SK, Pryor M, Sampson ML, Yang L, Freeman LA, Remaley AT, Creation of Apolipoprotein C-II (ApoC-II) Mutant Mice and Correction of Their Hypertriglyceridemia with an ApoC-II Mimetic Peptide. Journal of Pharmacology and Experimental Therapeutics356, 341–353 (2016)10.1124/jpet.115.229740).

16. MacRaild CA, Hatters DM, Howlett GJ, Gooley PR, NMR Structure of Human Apolipoprotein C-II in the Presence of Sodium Dodecyl Sulfate. Biochemistry40, 5414–5421 (2001); published online Epub2001/05/01 (10.1021/bi002821m). [PubMed: 11331005]

17. Segrest JP, Jones MK, De Loof H, Brouillette CG, Venkatachalapathi YV, Anantharamaiah GM, The amphipathic helix in the exchangeable apolipoproteins: a review of secondary structure and function. J Lipid Res33, 141–166 (1992); published online EpubFeb ([PubMed: 1569369]

18. Musliner TA, Herbert PN, Church EC, Activation of lipoprotein lipase by native and acylated peptides of apolipoprotein C-II. Biochim Biophys Acta573, 501–509 (1979); published online EpubJun 21 ([PubMed: 465517]

19. MacRaild CA, Howlett GJ, Gooley PR, The structure and interactions of human apolipoprotein C-II in dodecyl phosphocholine. Biochemistry43, 8084–8093 (2004); published online EpubJun 29 (10.1021/bi049817l). [PubMed: 15209504]

20. Anantharamaiah GM, Jones JL, Brouillette CG, Schmidt CF, Chung BH, Hughes TA, Bhown AS, Segrest JP, Studies of synthetic peptide analogs of the amphipathic helix. Structure of complexes

with dimyristoyl phosphatidylcholine. J Biol Chem260, 10248–10255 (1985); published online EpubAug 25 ([PubMed: 4019510]

21. Chung BH, Anatharamaiah GM, Brouillette CG, Nishida T, Segrest JP, Studies of synthetic peptide analogs of the amphipathic helix. Correlation of structure with function. J Biol Chem260, 10256–10262 (1985); published online EpubAug 25 ([PubMed: 4019511]
22. MacRaild CA, Hatters DM, Howlett GJ, Gooley PR, NMR structure of human apolipoprotein C-II in the presence of sodium dodecyl sulfate. Biochemistry40, 5414–5421 (2001); published online EpubMay 8 ([PubMed: 11331005]
23. Komatsu T, Sakurai T, Wolska A, Amar MJ, Sakurai A, Vaisman BL, Sviridov D, Demosky S, Pryor M, Ikewaki K, Remaley AT, Apolipoprotein C-II Mimetic Peptide Promotes the Plasma Clearance of Triglyceride-Rich Lipid Emulsion and the Incorporation of Fatty Acids into Peripheral Tissues of Mice. J Nutr Metab2019, 7078241 (2019)10.1155/2019/7078241). [PubMed: 30863636]
24. https://www.fresenius-kabi.com/en-ca/documents/Intralipid-PM-ENG.pdf, INTRALIPID® monograph. Fresenius Kabi Canada Ltd., (2017).
25. Sacks FM, The crucial roles of apolipoproteins E and C-III in apoB lipoprotein metabolism in normolipidemia and hypertriglyceridemia. Current Opinion in Lipidology26, 56–63 (2015)10.1097/MOL.0000000000000146). [PubMed: 25551803]
26. Ito Y, Azrolan N, O'Connell A, Walsh A, Breslow JL, Hypertriglyceridemia as a result of human apo CIII gene expression in transgenic mice. Science249, 790–793 (1990); published online EpubAug 17 ([PubMed: 2167514]
27. Gordts PL, Nock R, Son NH, Ramms B, Lew I, Gonzales JC, Thacker BE, Basu D, Lee RG, Mullick AE, Graham MJ, Goldberg IJ, Crooke RM, Witztum JL, Esko JD, ApoC-III inhibits clearance of triglyceride-rich lipoproteins through LDL family receptors. J Clin Invest126, 2855–2866 (2016); published online EpubAug 1 (10.1172/JCI86610). [PubMed: 27400128]
28. Thongtang N, Diffenderfer MR, Ooi EMM, Barrett PHR, Turner SM, Le NA, Brown WV, Schaefer EJ, Metabolism and proteomics of large and small dense LDL in combined hyperlipidemia: effects of rosuvastatin. J Lipid Res58, 1315–1324 (2017); published online EpubJul (10.1194/jlr.M073882). [PubMed: 28392500]
29. Zech LA, Schaefer EJ, Bronzert TJ, Aamodt RL, Brewer HB Jr., Metabolism of human apolipoproteins A-I and A-II: compartmental models. J Lipid Res24, 60–71 (1983); published online EpubJan ([PubMed: 6403641]
30. Matthan NR, Jalbert SM, Barrett PH, Dolnikowski GG, Schaefer EJ, Lichtenstein AH, Gender-specific differences in the kinetics of nonfasting TRL, IDL, and LDL apolipoprotein B-100 in men and premenopausal women. Arterioscler Thromb Vasc Biol28, 1838–1843 (2008); published online EpubOct (10.1161/ATVBAHA.108.163931). [PubMed: 18658047]
31. Amar MJ, D'Souza W, Turner S, Demosky S, Sviridov D, Stonik J, Luchoomun J, Voogt J, Hellerstein M, Sviridov D, Remaley AT, 5A apolipoprotein mimetic peptide promotes cholesterol efflux and reduces atherosclerosis in mice. J Pharmacol Exp Ther334, 634–641 (2010); published online EpubAug (10.1124/jpet.110.167890). [PubMed: 20484557]
32. Navab M, Anantharamaiah GM, Reddy ST, Hama S, Hough G, Grijalva VR, Yu N, Ansell BJ, Datta G, Garber DW, Fogelman AM, Apolipoprotein A-I mimetic peptides. Arterioscler Thromb Vasc Biol25, 1325–1331 (2005); published online EpubJul (10.1161/01.ATV.0000165694.39518.95). [PubMed: 15831812]
33. Camacho CJ, Katsumata Y, Ascherman DP, Structural and thermodynamic approach to peptide immunogenicity. PLoS Comput Biol4, e1000231 (2008); published online EpubNov (10.1371/journal.pcbi.1000231). [PubMed: 19023401]
34. Olivecrona G, Beisiegel U, Lipid binding of apolipoprotein CII is required for stimulation of lipoprotein lipase activity against apolipoprotein CII-deficient chylomicrons. Arterioscler Thromb Vasc Biol17, 1545–1549 (1997); published online EpubAug ([PubMed: 9301634]
35. Pollin TI, Damcott CM, Shen H, Ott SH, Shelton J, Horenstein RB, Post W, McLenithan JC, Bielak LF, Peyser PA, Mitchell BD, Miller M, O'Connell JR, Shuldiner AR, A null mutation in human APOC3 confers a favorable plasma lipid profile and apparent cardioprotection. Science322, 1702–1705 (2008); published online EpubDec 12 (10.1126/science.1161524). [PubMed: 19074352]

36. Klarin D, Damrauer SM, Cho K, Sun YV, Teslovich TM, Honerlaw J, Gagnon DR, DuVall SL, Li J, Peloso GM, Chaffin M, Small AM, Huang J, Tang H, Lynch JA, Ho YL, Liu DJ, Emdin CA, Li AH, Huffman JE, Lee JS, Natarajan P, Chowdhury R, Saleheen D, Vujkovic M, Baras A, Pyarajan S, Di Angelantonio E, Neale BM, Naheed A, Khera AV, Danesh J, Chang KM, Abecasis G, Willer C, Dewey FE, Carey DJ, Global Lipids Genetics C, Myocardial Infarction Genetics C, Geisinger-Regeneron Discov EHRC, Program VAMV, Concato J, Gaziano JM, O'Donnell CJ, Tsao PS, Kathiresan S, Rader DJ, Wilson PWF, Assimes TL, Genetics of blood lipids among ~300,000 multi-ethnic participants of the Million Veteran Program. Nat Genet50, 1514–1523 (2018); published online EpubNov (10.1038/s41588-018-0222-9). [PubMed: 30275531]

37. Graham MJ, Lee RG, Bell TA 3rd, Fu W, Mullick AE, Alexander VJ, Singleton W, Viney N, Geary R, Su J, Baker BF, Burkey J, Crooke ST, Crooke RM, Antisense oligonucleotide inhibition of apolipoprotein C-III reduces plasma triglycerides in rodents, nonhuman primates, and humans. Circ Res112, 1479–1490 (2013); published online EpubMay 24 (10.1161/CIRCRESAHA.111.300367). [PubMed: 23542898]

38. Gaudet D, Alexander VJ, Baker BF, Brisson D, Tremblay K, Singleton W, Geary RS, Hughes SG, Viney NJ, Graham MJ, Crooke RM, Witztum JL, Brunzell JD, Kastelein JJ, Antisense Inhibition of Apolipoprotein C-III in Patients with Hypertriglyceridemia. N Engl J Med373, 438–447 (2015); published online EpubJul 30 (10.1056/NEJMoa1400283). [PubMed: 26222559]

39. Pechlaner R, Tsimikas S, Yin X, Willeit P, Baig F, Santer P, Oberhollenzer F, Egger G, Witztum JL, Alexander VJ, Willeit J, Kiechl S, Mayr M, Very-Low-Density Lipoprotein-Associated Apolipoproteins Predict Cardiovascular Events and Are Lowered by Inhibition of APOC-III. J Am Coll Cardiol69, 789–800 (2017); published online EpubFeb 21 (10.1016/j.jacc.2016.11.065). [PubMed: 28209220]

40. Erkelens DW, Mocking JA, The CII/CIII ratio of transferable apolipoprotein in primary and secondary hypertriglyceridemia. Clin Chim Acta121, 59–65 (1982); published online EpubMay 6 ([PubMed: 7083594]

41. Beliard S, Nogueira JP, Maraninchi M, Lairon D, Nicolay A, Giral P, Portugal H, Vialettes B, Valero R, Parallel increase of plasma apoproteins C-II and C-III in Type 2 diabetic patients. Diabet Med26, 736–739 (2009); published online EpubJul (10.1111/j.1464-5491.2009.02757.x). [PubMed: 19573124]

42. Meyers NL, Larsson M, Olivecrona G, Small DM, A pressure-dependent model for the regulation of lipoprotein lipase by apolipoprotein C-II. Journal of Biological Chemistry290, 18029–18044 (2015)10.1074/jbc.M114.629865).

43. Gordon S, Durairaj A, Lu JL, Davidson WS, High-Density Lipoprotein Proteomics: Identifying New Drug Targets and Biomarkers by Understanding Functionality. Curr Cardiovasc Risk Rep4, 1–8 (2010)10.1007/s12170-009-0069-9). [PubMed: 20625533]

44. Gordon SM, Pourmousa M, Sampson M, Sviridov D, Islam R, Perrin BS, Kemeh G, Pastor RW, Remaley AT, Identification of a novel lipid binding motif in apolipoprotein B by the analysis of hydrophobic cluster domains. Biochim. Biophys. Acta1859, 135–145 (2017).

45. Brooks BR, Brooks CL 3rd, Mackerell AD Jr., Nilsson L, Petrella RJ, Roux B, Won Y, Archontis G, Bartels C, Boresch S, Caflisch A, Caves L, Cui Q, Dinner AR, Feig M, Fischer S, Gao J, Hodoscek M, Im W, Kuczera K, Lazaridis T, Ma J, Ovchinnikov V, Paci E, Pastor RW, Post CB, Pu JZ, Schaefer M, Tidor B, Venable RM, Woodcock HL, Wu X, Yang W, York DM, Karplus M, CHARMM: the biomolecular simulation program. Journal of computational chemistry30, 1545–1614 (2009); published online EpubJul 30 (10.1002/jcc.21287). [PubMed: 19444816]

46. Masucci-Magoulas L, Goldberg IJ, Bisgaier CL, Serajuddin H, Francone OL, Breslow JL, Tall AR, A mouse model with features of familial combined hyperlipidemia. Science275, 391–394 (1997); published online EpubJan 17 ([PubMed: 8994037]

47. Noh HL, Okajima K, Molkentin JD, Homma S, Goldberg IJ, Acute lipoprotein lipase deletion in adult mice leads to dyslipidemia and cardiac dysfunction. Am J Physiol Endocrinol Metab291, E755–760 (2006); published online EpubOct (10.1152/ajpendo.00111.2006). [PubMed: 16684851]

48. Micsonai A, Wien F, Bulyaki E, Kun J, Moussong E, Lee YH, Goto Y, Refregiers M, Kardos J, BeStSel: a web server for accurate protein secondary structure prediction and fold recognition

from the circular dichroism spectra. Nucleic Acids Res46, W315–W322 (2018); published online EpubJul 2 (10.1093/nar/gky497). [PubMed: 29893907]

49. Best RB, Zhu X, Shim J, Lopes PE, Mittal J, Feig M, MacKerell AD Jr, Optimization of the additive CHARMM all-atom protein force field targeting improved sampling of the backbone φ, ψ and side-chain χ1 and χ2 dihedral angles. J. Chem. Theory Comput. 8, 3257 (2012). [PubMed: 23341755]
50. Klauda JB, Venable RM, Freites JA, O'Connor JW, Tobias DJ, Mondragon-Ramirez C, Vorobyov I, MacKerell AD Jr., Pastor RW, Update of the CHARMM all-atom additive force field for lipids: validation on six lipid types. J Phys Chem B114, 7830–7843 (2010)10.1021/jp101759q). [PubMed: 20496934]
51. Jorgensen WL, Chandrasekhar J, Madura JD, Impey RW, Klein ML, Comparison of simple potential functions for simulating liquid water. J. Chem. Phys. 79, 926–935 (1983).
52. Venable RM, Luo Y, Gawrisch K, Roux B, Pastor RW, Simulations of anionic lipid membranes: Development of interaction-specific ion parameters and validation using NMR data. J. Phys. Chem. B117, (2013).
53. Feller SE, Zhang Y, Pastor RW, Brooks BR, Constant pressure molecular dynamics simulation: The Langevin piston method. 103, 4613–4621 (1995)10.1063/1.470648).
54. Lippert RA, Predescu C, Ierardi DJ, Mackenzie KM, Eastwood MP, Dror RO, Shaw DE, Accurate and efficient integration for molecular dynamics simulations at constant temperature and pressure. The Journal of Chemical Physics139, 164106 (2013); published online EpubOct 28 (10.1063/1.4825247). [PubMed: 24182003]
55. Kräutler V, A fast SHAKE algorithm to solve distance constraint equations for small molecules in molecular dynamics simulations. Journal of computational chemistry22, 501–508 (2001).
56. de Messieres M, Huang RK, He Y, Lee JC, Amyloid triangles, squares, and loops of apolipoprotein C-III. Biochemistry53, 3261–3263 (2014); published online EpubMay 27 (10.1021/bi500502d). [PubMed: 24804986]
57. Freeman LA, Lipoproteins and Cardiovascular Disease. Methods in Molecular Biology (Methods and Protocols). Humana Press, Totowa, NJ, 1027, (2013)10.1007/978-1-60327-369-5_18).

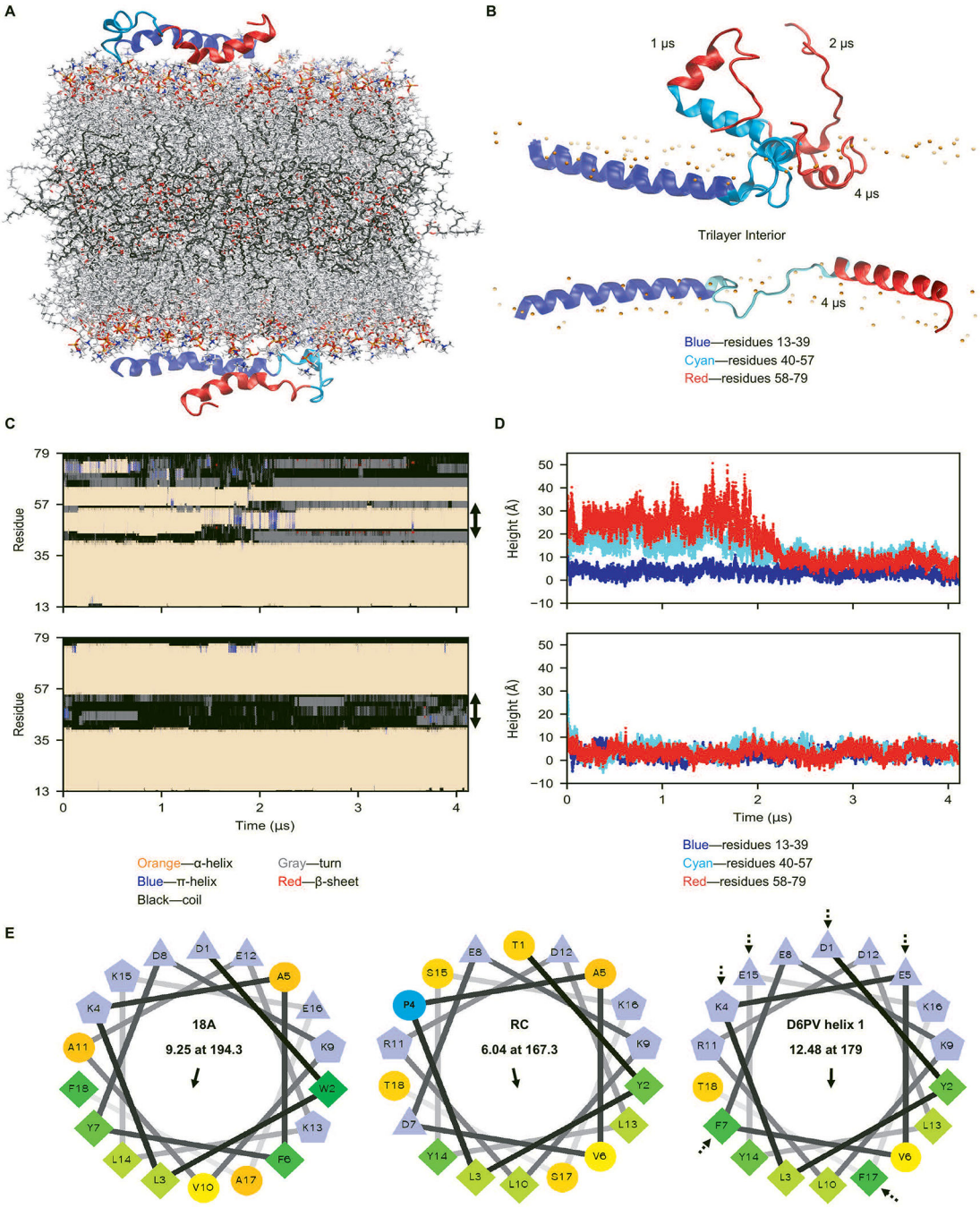

Fig 1. MD simulation of apoC-II and peptide design.

(A) Initial configuration of MD simulation of apoC-II interacting with a lipid trilayer composed of a layer of TG surrounded by two layers of POPC. Proteins are shown as ribbons with residues 13–39, 40–57, and 58–79 in blue, cyan, and red, respectively. POPC and TG are shown as sticks (phosphorus, orange; oxygen, red; nitrogen, blue; carbons of POPC, gray; carbons of TG, black). **(B)** Simulation snapshots of two copies of apoC-II. The structures of N-terminal region of the top apoC-II at 1 μs, 2 μs, and 4 μs are superimposed to show the mobility of the rest of the protein. Phosphorus atoms of POPC are shown as orange

spheres. **(C)** Time series of secondary structures of two copies of apoC-II. The central, non-helical region is indicated by arrow. Color code: α-helix, orange; π-helix, blue; coil, black; turn, gray; β-sheet, red. **(D)** Time series of the height of residues 13–39 (blue), 40–57 (cyan), and 58–79 (red) of the two copies of apoC-II above the C2 atoms of *sn*-2 chains of lipids. Negative values indicate insertion into the hydrophobic region of lipids. **(E)** Helical wheel plots of 18A, random coil (RC) region of apoC-II, and helix 1 of D6PV. Red arrows show site of amino acid residue substitutions for helix 1. First number in the center of the helical wheel indicates hydrophobic moment. Second number in the center of the helical wheel and black arrow indicate angle of hydrophobic moment.

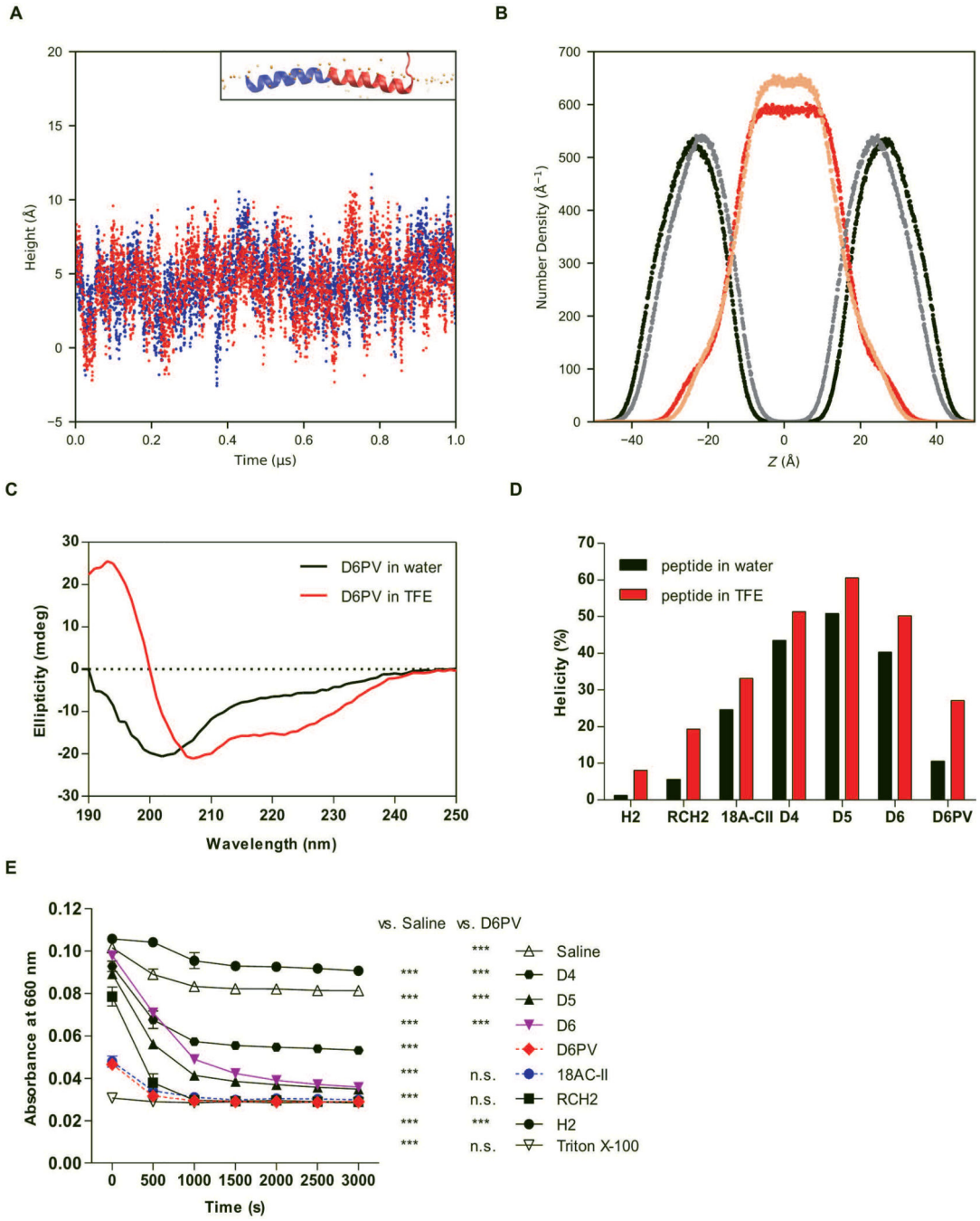

Fig. 2. MD simulation of D6PV and peptide physical characterization.

(A) Time series of the height of the N-terminal (blue) and the C-terminal (red) of one copy of D6PV above the C2 atoms of *sn*-2 chains of lipids. Data corresponding to the copy of D6PV on the other leaflet is not presented for clarity. Negative values indicate insertion into the hydrophobic region of lipids. Inset shows the average structure of D6PV with N- and C-terminals colored in blue and red, respectively. **(B)** Number density of POPC and TG molecules along the direction perpendicular to the lipid trilayer surface (*z*-axis) in two systems: D6PV-free lipid trilayer (POPC: black; TG: red) and D6PV-associated lipid

trilayer (POPC: gray; TG: orange). **(C)** CD spectrum of D6PV in water (black) or 10% TFE (red). **(D)** Percent helicity of apoC-II mimetic peptides and truncated forms of native apoC-II. **(E)** Effect of the apoC-II mimetic peptides and truncated forms of apoC-II on solubilization of DMPC vesicles. A homogenous vesicle solution of DMPC (0.15 mg/mL, in PBS) was incubated with Triton X-100 (positive control), buffer saline (negative control), truncated forms of apoC-II (0.1 mg/mL), and apoC-II mimetic peptides (0.1 mg/mL). Results represent the mean of triplicates ± S.D. Two-way ANOVA and Bonferroni post-test were used to compare means of the different treatments at each time point, *** $P < 0.001$; *n.s.* ($P > 0.5$), comparison to saline or D6PV.

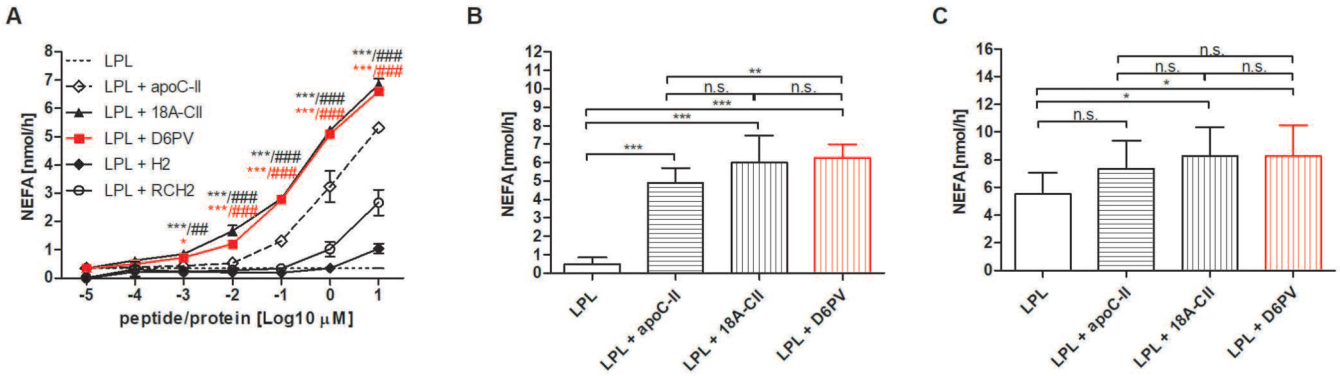

Fig. 3. Effect of D6PV on TG lipolysis in human HTG plasma.

(A) Efficiency of TG lipolysis in human plasma after addition of LPL and apoC-II, the C-terminal helix of apoC-II (H2), the random coil region with the C-terminal helix of apoC-II (RCH2), 18A-CII, or D6PV (in red) to human apoC-II-deficient plasma (TG=1711 mg/dL) at indicated concentrations. Results represent the mean of triplicates ± S.D. Two-way ANOVA test and Bonferroni post-test to compare means at the different concentrations versus LPL (* $P < 0.05$, *** $P < 0.001$) or versus LPL + apoC-II (## $P < 0.01$, ### $P < 0.001$). **(B)** Lipolysis after adding LPL and apoC-II, 18A-CII, or D6PV (10 µM, each) to human apoC-II-deficient plasma (TG=1711 mg/dL). Results represent the mean ± S.D., N=8; Mann-Whitney test, ** $P < 0.01$, *** $P < 0.001$. **(C)** Lipolysis after adding LPL and apoC-II, 18A-CII, or D6PV (10 µM, each) to pooled human HTG plasma (TG=300–600 mg/dL). Results represent the mean ± S.D., N=8; Mann-Whitney test, * $P < 0.05$.

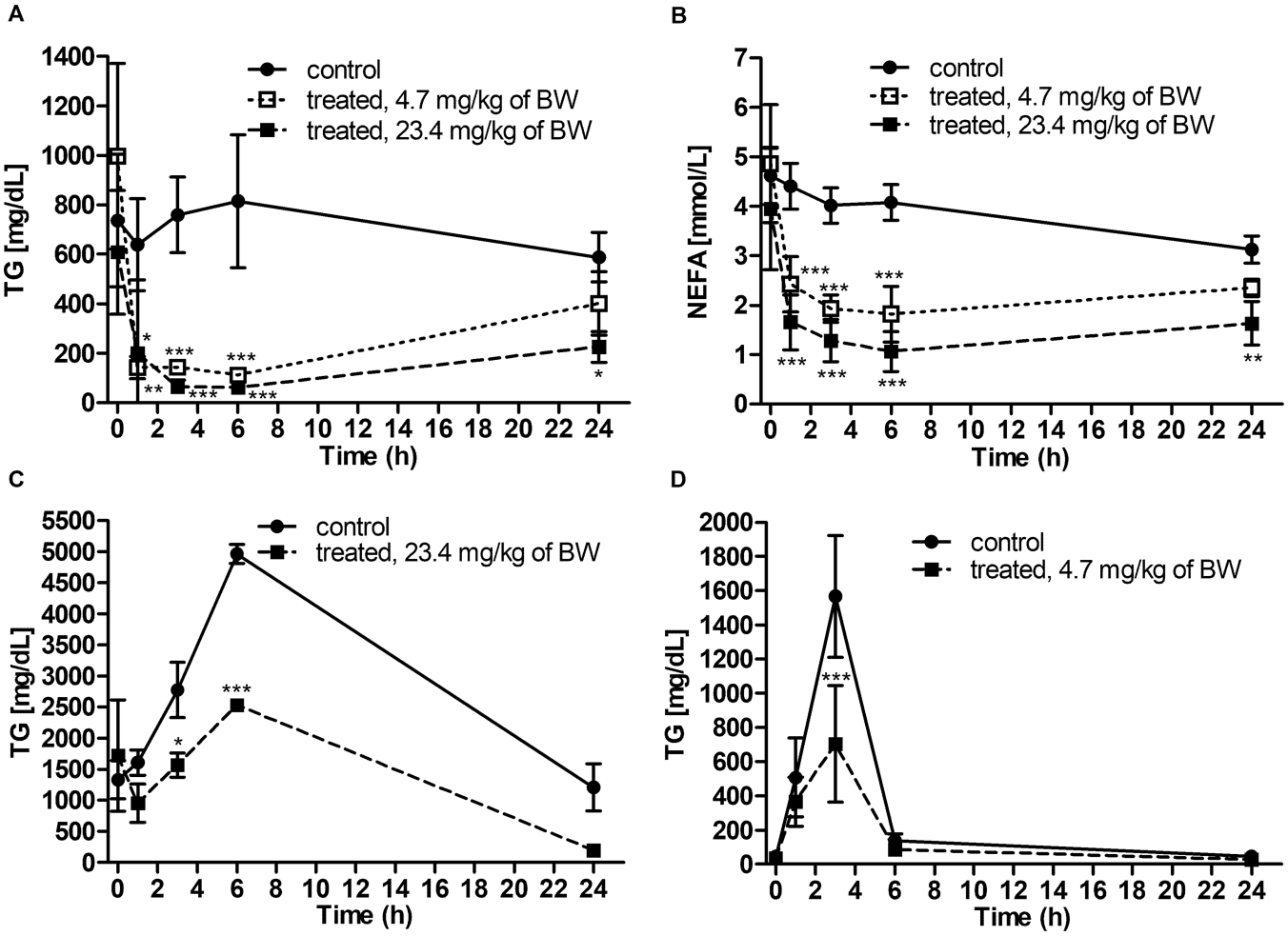

Fig. 4. Effect of D6PV on TG lipolysis in human HTG mouse models.

(A) Efficiency of TG lipolysis in plasma of apoC-II-deficient mice injected with a single IP bolus of either vehicle (control) or D6PV (treated; 4.7 mg/kg or 23.4 mg/kg), N=12. **(B)** NEFA concentrations in plasma of apoC-II-deficient mice injected with a single IP bolus of either vehicle (control) or D6PV (treated; 4.7 mg/kg or 23.4 mg/kg), N=12. **(C)** TG lipolysis in the plasma of apoC-II-deficient mice first injected IP with a 1 mL bolus of 20% Intralipid and then a single IP bolus of either vehicle (control) or D6PV (treated; 23.4 mg/kg), N=6. **(D)** TG lipolysis in plasma of C57Bl/6 mice first injected IP with a 0.6 mL bolus of 20% Intralipid and then a single IP bolus of either vehicle (control) or D6PV (treated; 23.4 mg/kg), N=6. Results represent the mean ± S.D. Two-way ANOVA test and Bonferroni post-test to compare means at the different time points versus vehicle control groups. * $P < 0.05$, ** $P < 0.01$, *** $P < 0.001$.

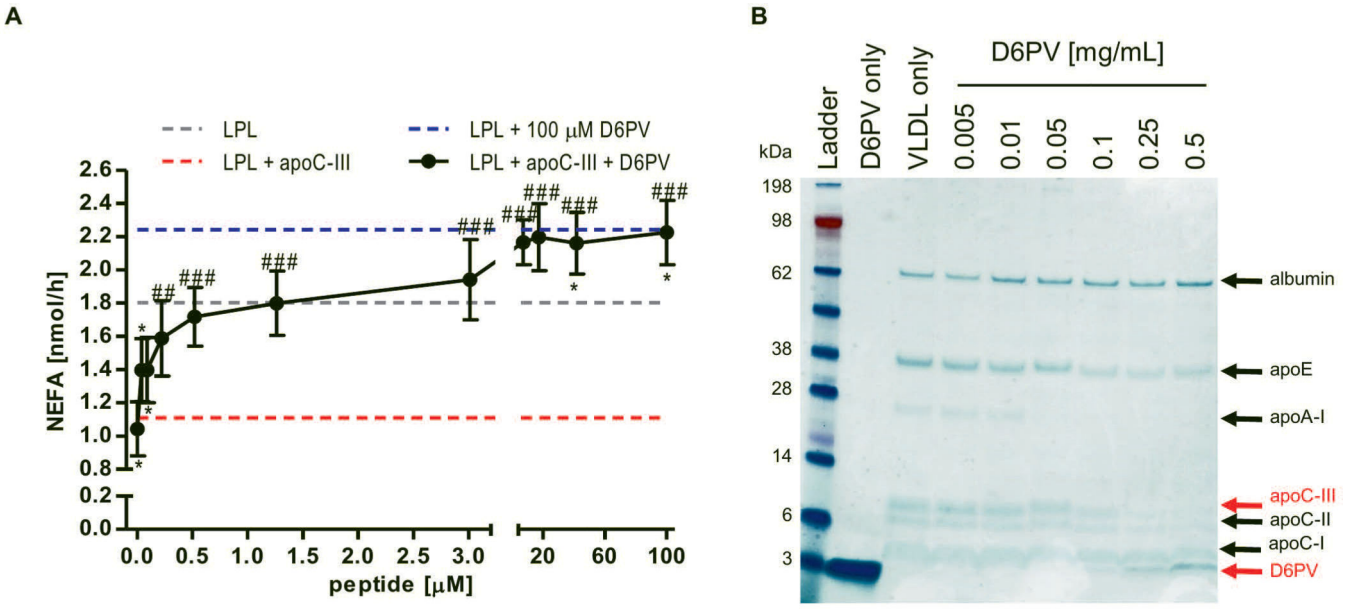

Fig. 5. Effect of D6PV on human apoC-III and LPL activity.

(A) Effect of D6PV on TG lipolysis in the presence of apoC-III added to pooled human HTG plasma. LPL was added to plasma (TG=360 mg/dL) and incubated in the presence of increasing concentrations of D6PV, in a dose from 0–100 µM (0–0.47 mg/mL) with and without 33 µM apoC-III. LPL alone established baseline lipolysis (gray), whereas LPL and 100 µM D6PV established maximum uninhibited lipolysis (blue) and LPL with 33 µM apoC-III established maximum inhibited lipolysis (red). Results represent the mean of triplicates ± S.D. Two-way ANOVA test and Bonferroni post-test to compare means at the different peptide concentration, * $P < 0.05$ compared with LPL only; ## $P < 0.01$ compared with LPL with apoC-III; ### $P < 0.001$ compared with LPL with apoC-III. **(B)** Human VLDL were incubated with the indicated concentration of D6PV for 1 h at 37°C. Displaced apolipoproteins were removed using spin filters (100-kDa cutoff) and VLDL-bound proteins were separated by electrophoresis and identified by MALDI-TOF.

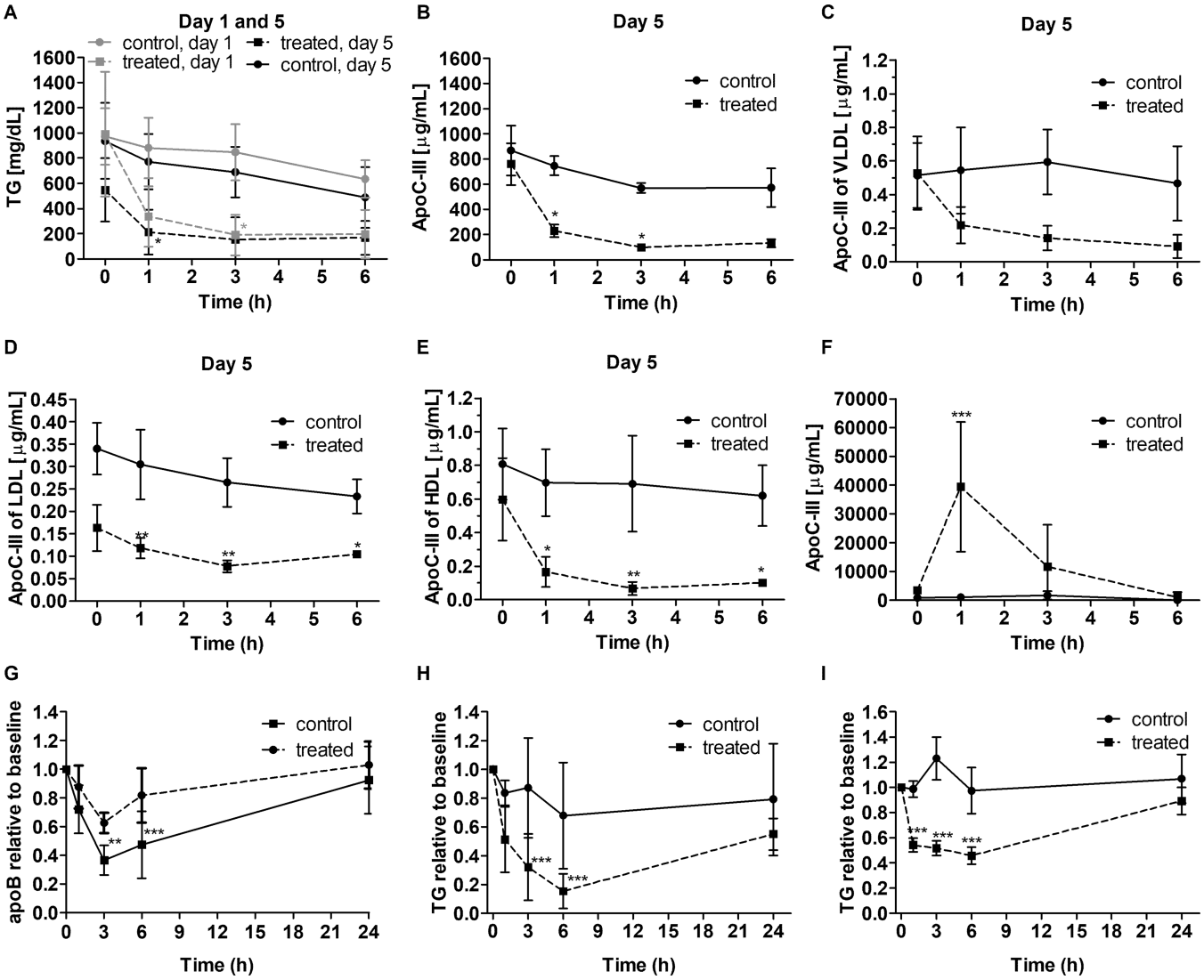

Fig. 6. Effect of D6PV on TG, apoC-III and apoB in mouse models for HTG.

(A-E) h*APOC3*-Tg mice were injected daily with a single IV bolus of either vehicle (control) or D6PV (treated; 23.4 mg/kg) for 5 days, N=6. Blood samples for analysis were obtained at the indicated day and time after injection. **(A)** Plasma TG concentrations on day 1 (gray) and day 5 (black) of the 5-day study. **(B)** Plasma apoC-III concentrations on day 5. **(C)** ApoC-III of plasma VLDL on day 5. **(D)** ApoC-III of plasma LDL on day 5. **(E)** ApoC-III of plasma HDL on day 5. **(F)** ApoC-III concentrations in urine of h*APOC3-Tg* mice after a single IV bolus injection of either vehicle (control) or D6PV (treated; 23.4 mg/kg), N=7. **(G)** Plasma apoB in h*APOC3*-Tg mice after a single IV bolus of either vehicle (control) or D6PV (treated; 23.4 mg/kg), N=20. Results are presented as apoB relative to baseline; mean plasma apoB concentrations for control and treated mice were 31 and 33 mg/dL, respectively. **(H)** Plasma TG in h*APOC3*-Tg x $Ldlr^{-/-}$ mice injected with a single IP bolus of either vehicle (control) or D6PV (treated; 23.4 mg/kg), N=18. Results are presented as TG relative to baseline; mean plasma TG concentrations for control and treated mice were 1727 and 1734 mg/dL, respectively. **(I)** Plasma TG in i$Lpl^{-/-}$ mice injected with a single IV

bolus of either vehicle (control) or D6PV (treated; 23.4 mg/kg), N=14. Results are presented as TG relative to baseline; mean plasma TG concentrations for control and treated mice were 364 and 449 mg/dL, respectively. Results represent the mean ± S.D. Two-way ANOVA test and Bonferroni post-test to compare means at the different time points versus vehicle control groups. * $P < 0.05$, ** $P < 0.01$, *** $P < 0.001$.

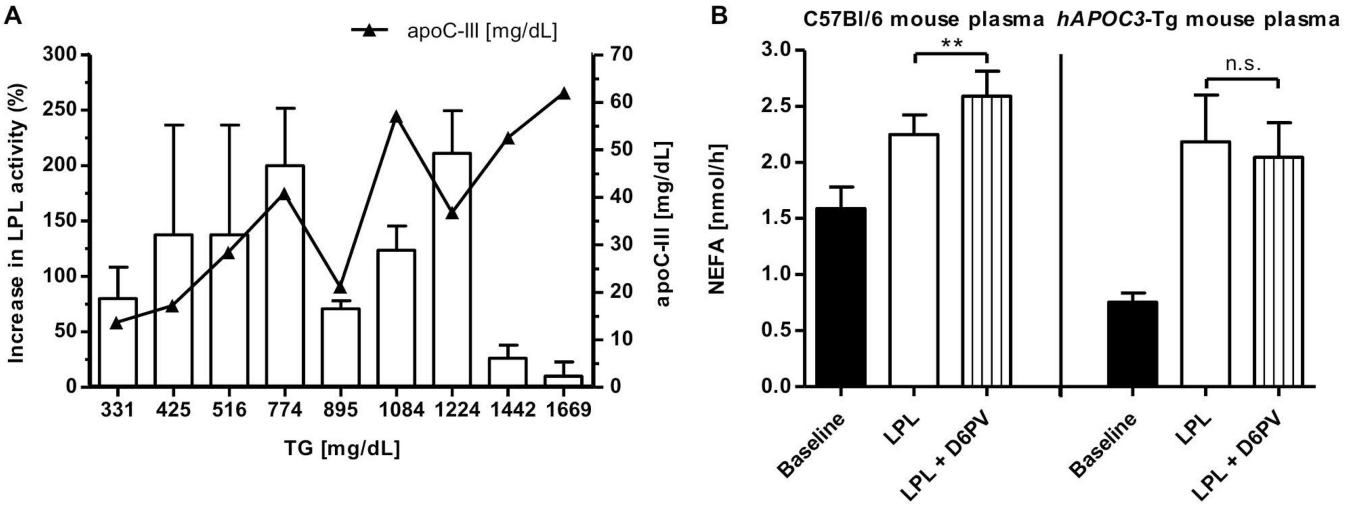

Fig. 7. Effect of D6PV on TG lipolysis in HTG plasma.

Effect of D6PV on TG lipolysis in **(A)** plasma from patients with HTG and various concentrations of apoC-III, N=9. Bars represent increase in LPL activity (%) and triangle symbols represent plasma apoC-III concentrations [mg/dL]. **(B)** NEFA concentration in C57Bl/6 and h*APOC3*-Tg mouse plasma treated with LPL and D6PV, N=6. Results represent the mean ± S.D, Mann-Whitney test. *n.s.* compared with h*APOC3*-Tg mouse plasma treated with LPL only; ** $P < 0.01$ compared with C57Bl/6 mouse plasma treated with LPL only.

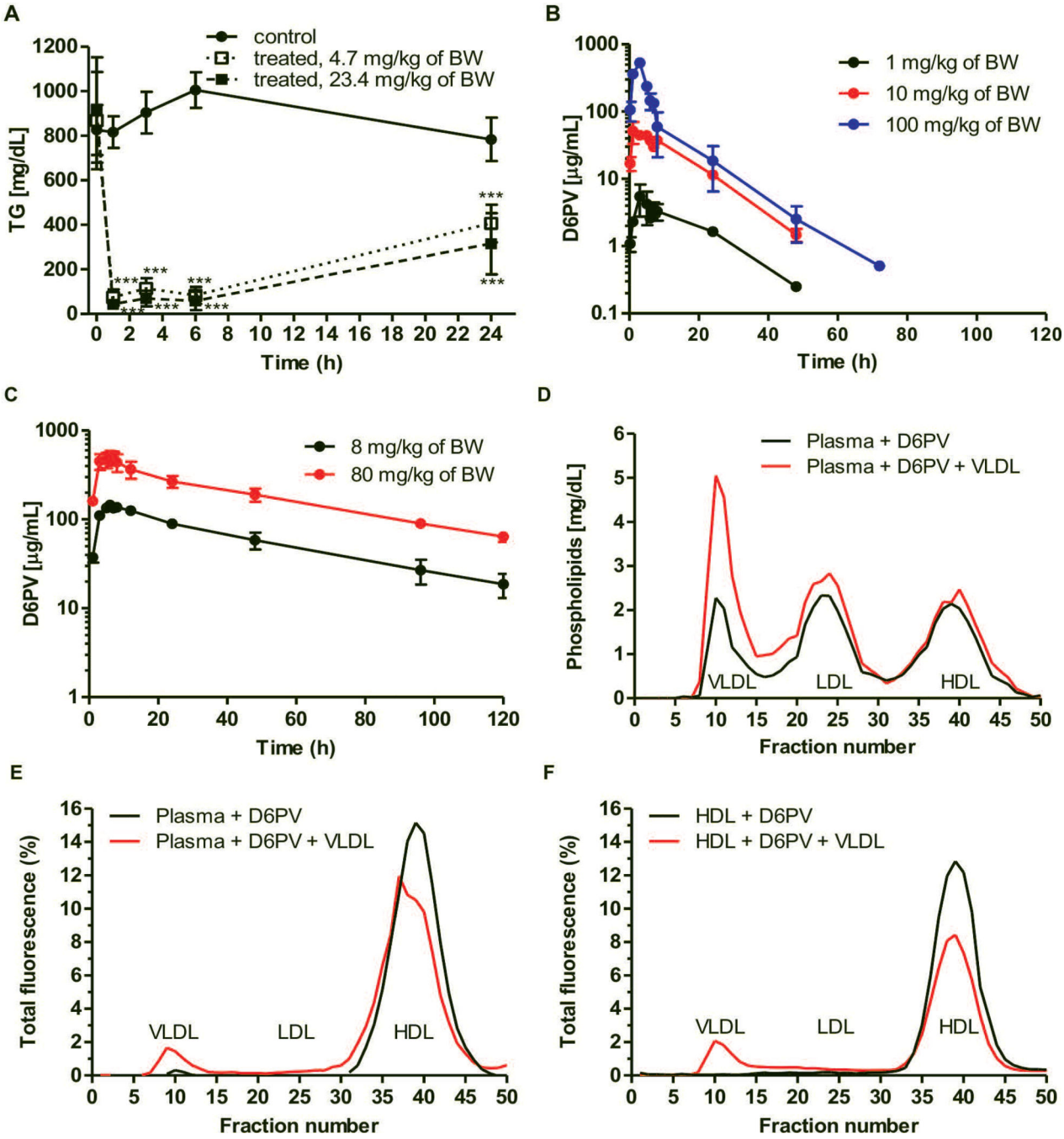

Fig. 8. Pharmacokinetics and lipoprotein binding properties of D6PV.

(A) Plasma TG in apoC-II-deficient mice injected subcutaneously with a single bolus of either vehicle (control) or D6PV (treated; 4.7 mg/kg or 23.4 mg/kg), N=12. Results represent the mean ± S.D. Two-way ANOVA test and Bonferroni post-test to compare means at the different time points versus vehicle control. *** $P < 0.001$. **(B)** PK results of C57Bl/6 mice injected subcutaneously with a single dose of D6PV at 1, 10, and 100 mg/kg. **(C)** PK results of nonhuman primates injected subcutaneously with a single dose of D6PV at 8 and 80 mg/kg. **(D)** Phospholipid distribution of lipoproteins separated by FPLC from

pooled human HTG (TG=360 mg/dL) plasma supplemented with either PBS or VLDL (0.15 mg/mL of protein) and incubated with 0.3 mg/mL D6PV-5-TAMRA for 30 min. **(E)** Percent of total fluorescence of D6PV on lipoproteins from pooled human HTG (TG=360 mg/dL) plasma supplemented with either PBS or VLDL shown in panel D. **(F)** Percent of total fluorescence of D6PV on lipoproteins after co-incubation of purified HDL (0.25 mg/mL of protein) pre-labelled with D6PV-5-TAMRA with either human VLDL (0.15 mg/mL of protein) or PBS for 30 min at 37°C.

Table 1.

Sequences of apoC-II mimetic peptides.

apoC-II residue #	40	41	42	43	44	45	46	47	48	49	50	51	52	53	54	55	56	57	58	59	60	61	62	63	64	65	66
peptide residue #	1	2	3	4	5	6	7	8	9	10	11	12	13	14	15	16	17	18	19	20	21	22	23	24	25	26	27
H2																				A	M	S	T	Y	T	G	I
RCH2	T	Y	L	P	A	V	D	E	K	L	R	D	L	Y	S	K	S	T	A	A	M	S	T	Y	T	G	I
18A-CII	D	W	L	K	A	F	Y	D	K	V	A	E	K	L	K	E	A	F	P	A	M	S	T	Y	T	G	I
D4	D	Y	L	K	A	V	F	E	K	L	R	D	L	Y	S	K	F	T	A	A	nL	S	T	Y	T	G	I
D5	D	Y	L	K	E	V	F	E	K	L	R	D	L	Y	S	K	F	T	A	A	nL	S	T	Y	T	G	I
D6	D	Y	L	K	E	V	F	E	K	L	R	D	L	Y	E	K	F	T	A	A	nL	S	T	Y	T	G	I
D6PV	D	Y	L	K	E	V	F	E	K	L	R	D	L	Y	E	K	F	T	P	A	V	S	T	Y	T	G	I

H2 – C-terminal helix of native apoC-II (residues 59–79). RCH2 – random coil region and C-terminal helix of native apoC-II (residues 40–79). Residues in the table: lysine (K), arginine (R), aspartic acid (D), glutamic acid (E), serine (S), threonine (T), glutamine (Q), alanine (A), valine (V), leucine (L), isoleucine (I), methionine (M), norleucine (nL), phenylalanine (F), tyrosine (Y), tryptophan (W), proline (P), glycine (G). Residues for native apoC-II are numbered according to their position in mature form of human apoC-II with 79 amino acids following cleavage of 22-amino acid signal peptide. Residues substituted in peptides from RCH2 are shown in red.

Table 2.

Physical properties of the apoC-II mimetic peptides and truncated forms of native apoC-II.

Peptide	MW (g/moL)	Net Charge (pH=7)	PI (pH)	Extinction Coefficient ($M^{-1}cm^{-1}$)	Hydrophobicity (%)	$\Delta G_{transfer}$ (kcal/moL)d	Depth/ Hydrophobic Thickness (Å)	Tilt Angle (°)
H2	2289.6	−2	3.69	1280	38.1	−4.0	5.8 ± 1.5	61 ± 9
RCH2	4422.0	−2	4.25	3840	37.5	−8.7	2.7 ± 1.3	69 ± 9
18A-CII	4570.2	−2	4.38	8250	45.0	−4.0	2.3 ± 1.2	70 ± 14
D4	4561.1	−1	4.67	3840	39.0	−14.2 *	7.6 ± 1.0 *	84 ± 7 *
D5	4619.2	−2	4.38	3840	36.6	−12.6 *	9.1 ± 1.3 *	81 ± 8 *
D6	4661.2	−3	4.22	4661	36.6	−12.3 *	7.3 ± 0.8 *	82 ± 7 *
D6PV	4673.2	−3	4.22	3840	37.5	−5.4	5.7 ± 0.7	58 ± 7

Calculated physical properties of the apoC-II mimetic peptides and truncated sequences of native apoC-II, the C-terminal helix of apoC-II (H2) and the random coil region with the C-terminal helix of apoC-II (RCH2).

*Peptides D4, D5, and D6 contain a non-natural amino acid, norleucine (nL), that could not be modeled by Pepfold3; therefore, the first 20 amino acids were used to model the structure of D4, D5, and D6; values determined by the OPM Database are based upon the partial models.